ChemComm

Accepted Manuscript

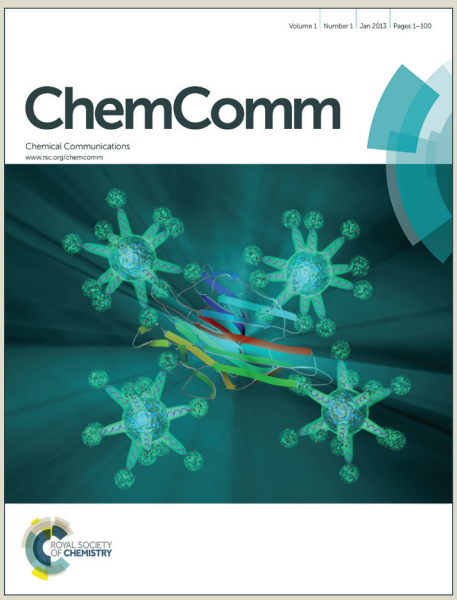

ROYAL SOCIETY OF CHEMISTRY

www.rsc.org/chemcomm

Journal Name

RSCPublishing

COMMUNICATION

Rutile TiO_2 Nanowires Perovskite Solar Cells

Y7uuhioiuuhyrt6t6r5Cite this: DOI: 10.1039/x0xx00000x

Qinglong Jiang[a], Xia Sheng[b], Yingxuan Li[c], Xinjian Feng[*a, b], Tao Xu[*a]

Received ooth January 20xx,
Accepted ooth January 20xx

DOI: 10.1039/x0xx00000x

www.rsc.org/

Abstract: Different lengths of rutile TiO_2 nanowires (NW) with wide-open space for effective material filling were used as photoanodes for perovskite solar cells. Cells with 900 nm nanowires as photoanodes exhibit current density of 22 mA/cm^2 and efficiency of 11.7%, exceeding the reported TiO_2 nanowire-based perovskite solar cells.

Since it was first reported in 2009,[1] perovskite type $CH_3NH_3PbX_3$ solid solar cells have recently been reported with over 15% efficiency.[2, 3, 4] The astounding improvements in efficiency achieved in the past few years suggests that it is a promising candidate for the next generation solar cells. This material exhibits unusual excellence in both charge transport (electron/hole diffusion lengths are about 1μm/1.2um $CH_3NH_3PbI_{3-X}Cl_x$, respectively[5]), and light harvesting (1.5×10^4 cm^{-1} at 550 nm).[6] In general, perovskite solar cells are configured as a sandwich structure. Explicitly, a mesostructured TiO_2 layer on FTO serves as the photoanode, which is filled up with perovskite $CH_3NH_3PbX_3$ as PV active layer, followed by capping with a hole transport material layer (HTM) and a metal counter electrode. It is noticed that the morphology, thickness and crystallinity of the TiO_2 layers,[7,8] including both the compact electron-blocking layer and the mesostructured layer,[4, 9] play a crucial role in the efficiency of similarly solar cells. For example, in dye sensitized solar cells, mesoporous TiO_2 films often suffer from the difficulty in filling of dye molecules in the highly convoluted porous channels.[10] This is also a problem with perovskite $CH_3NH_3PbX_3$.[11] On the other hand, electron diffusion length in $CH_3NH_3PbI_3$ is about 100 nm,[5] not thick enough to suffice light harvesting. For instance, when the thickness of mesoporous TiO_2 exceeds 600 nm, the electron/hole transport encounters large resistance, resulting in significant loss of open-circuit voltage (V_{oc}) and fill factor (FF).[6] Thus, the optimized thickness for mesoporous TiO_2 must be controlled in range of 400 nm to 600 nm.[3, 12-14]

The use of aligned array of one dimensional TiO_2 NWs as photoanode in perovskite solar cells provides a potential solution to the conflicting demands on light absorption and charge transport appeared in mesoporous photoanodes. As depicted in Figure 1, on one hand, the high electron diffusion length in the NWs facilitate/afford directed electron transport in the case of thick $CH_3NH_3PbI_3$ layer.[15] On the other hand, if the voids between the NWs is widely open, the filling of the perovskite solution can be much efficient than the compact NWs, forming a perovskite layer with nearly no dead volumes. Indeed, perovskite solar cell with one dimensional TiO_2 NWs array has reach 4.9% efficiency in the early stage,[15] and shortly, the efficiency achieved 9.4% using a rutile compact TiO_2 nano-rods structure, which is so far the highest efficiency achieved on NW-based perovskite cells.[16] Both reported TiO_2 NWs used in these previous works are all prepared via hydrothermal method.

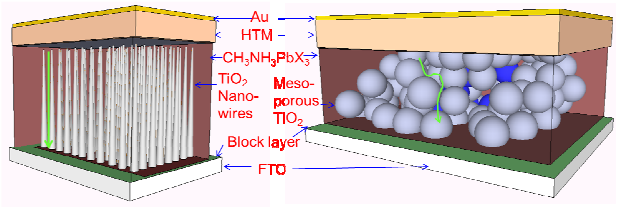

Figure 1. Schematic comparison between NWs TiO_2 and mesoporous TiO_2 photoanodes. Perovskite $CH_3NH_3PbX_3$ precursor and HTM filling paths were indicated in green for the nanowire photoanodes. In contrast, mesoporous photoanodes inevitably contains some dead volumes (blue parts) that are not readily accessible for the perovskite materials.

Recently, we reported a solvothermal method for the synthesis of rutile NWs with controllable length-to-diameter ratio and well-separated wire-to-wire space. We have also demonstrated that electron transport in these rutile NWs is 200 time faster than that of mesoporous rutile films[17]. Herein, we apply these rutile NW arrays with different length as photoanodes in perovskite solar cells and we achieved 11.7% efficiency, which is 2% (absolution value) higher than the best perovskite solar cells using nanowire as photoanode reported in the literatures.[16]

The synthesis of rutile TiO_2 NWs on FTO glass was reported earlier, which is also briefly described in supporting information.[17] The voids between the NWs are filled with a layer of spinning-coated $CH_3NH_3PbI_3$, followed by about 220 nm-thick

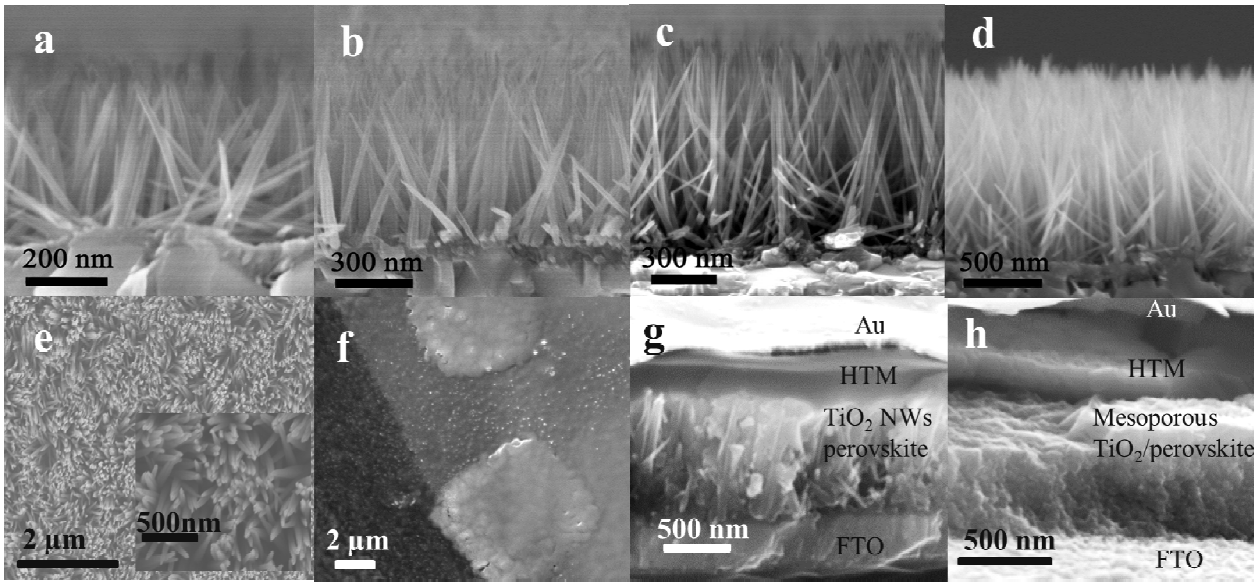

Figure 2. SEM images of TiO_2 NWs and solar cells. a. 400 nm NWs; b. 600 nm NWs; c. 900 nm NWs; d. 1.2 μm NWs; e. top view of 900 nm TiO_2 NWs; f. top view of solar cell; g. cross section of solar cell with 900 nm NWs as photoanode; h. cross section of solar cell with mesoporous TiO_2 as photoanode.

spinning-coated spiro-MeOTAD (2,2′ 7,7′ -tetrakis-(N,N-di-p-methoxyphenyl amine)-9,9′ -spirobifluorene as hole transport layer. Finally, a thermally evaporated gold layer (80 nm) is deposited as the cathode.

Figure 2a, 2b, 2c and 2d are the cross-section SEM images of 400 nm, 600 nm, 900 nm and 1.2 μm NWs on FTO, respectively. It can be seen that the NWs are 30~50 nm apart from each other, providing the voids for the filing of perovskite $CH_3NH_3PbI_3$ precursor. The top view of the 900 nm NWs (Figure 2e) further confirms that the voids among the NWs are open and accessible. According SEM images, the density of the rutile NWs is ~90/μm^2. Figure 2f is the SEM topview image around the edge of the gold electrode after filling of perovskite in the voids of the TiO_2 NWs and thermal deposition of gold counter electrodes. The brighter part is the thermally deposited gold electrode in comparison to the dark part that is not coated with gold. Apparently, no NWs or open space can be observed from top, indicating a good filling of $CH_3NH_3PbI_3$. The cross-section SEM image the device (Figure 2g) also manifests the tight filling of the $CH_3NH_3PbI_3$ in the wire-to-wire voids. Element analysis by energy dispersive spectrometer (EDS) also confirms the existence of $CH_3NH_3PbI_3$ with 3:1 atomic ratio between I and Pb (See Fig. S1 in ESI). In comparison, we also prepared cells with about 500 nm thick and 16-36 nm particles size mesoporous anatase TiO_2 as photoanode,[18] which is known to be the best optimized thickness for mesoporous TiO_2-based perovskite cells.[6] Figure 2h shows the cross section SEM image of the mesoporous TiO_2 cells.

X-ray Diffraction (XRD) of TiO_2 rutile NWs on fluorine doped tin oxide (FTO) substrate was shown in Figure 3. Peaks from FTO are indicated by triangles. Peak (101) along with the enhanced (002) peak in the NWs suggests that the rutile crystal grows with (101) plane parallel to the FTO substrate and the NWs are oriented along the (002) direction.[16, 19] The high resolution transmission electron microscope (HRTEM) image (Inset Figure 3) suggests the feature of the NWs. The (110) lattice crystal plane with a fringe spacing of 0.325 nm indicates that these nanowires are rutile TiO_2.

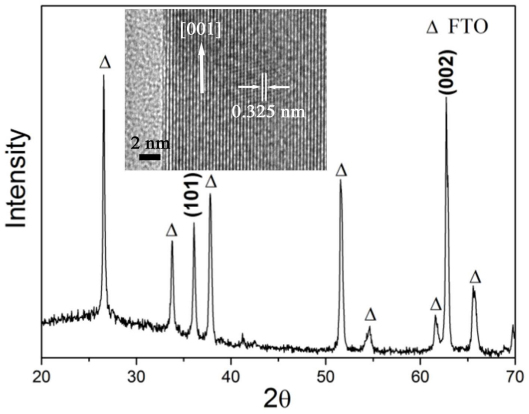

Figure 3. XRD and HR-TEM of TiO_2 NWs on FTO substrate.

Figure 4 exhibits J-V curves of the prepared NWs perovskite solar cells with different length of TiO2 NWs along with the dark current curves appeared as dash lines. The photovoltaic performances for all the solar cells are summarized in Table 1.

Cells with 900 nm TiO_2 NWs as photonanodes give the best efficiency of 11.7% followed by 600 nm TiO_2 NWs and 400 nm TiO_2 NWs with efficiency of 10.8% and 9.7%, respectively. For cells using 1.2 μm TiO_2 NWs as photonanode, the efficiency encounters a significant drop to only 4.8%. In terms of photocurrent density (J_{sc}), it increases as the length of NWs from 400nm (18.6 mA/cm^2) to 600 nm (20.4 mA/cm^2), to 900nm (22.3 mA/cm^2). It is worth to note that the efficiency of our 900nm TiO_2 NWs-based $CH_3NH_3PbI_3$ perovskite cells outperforms the best reported TiO_2 NWs-based perovskite solar cells in literature by 2% (absolute),[16] and the enhancement is mainly contributed from the elevated J_{sc} in our 900 nm NWs cells(7 mA/cm^2 greater than the best reported cells). As the length of TiO_2 NWs reaches 1.2 μm, however, J_{sc} decreases significantly to only 9.3 mA/cm^2, leading to the large drop inefficiency to only 4.8%.

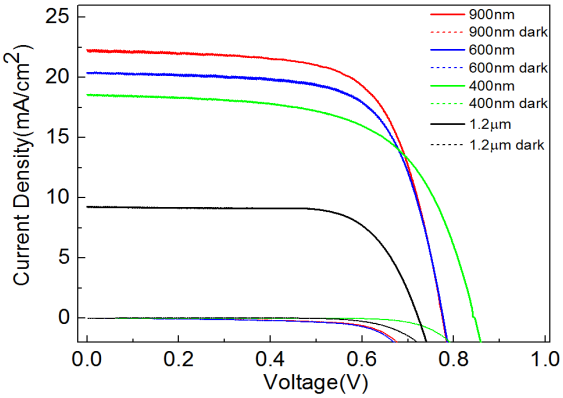

Figure 4. J-V curves of perovskite solar cell with 400 nm, 600 nm, 900 nm and 1.2 μm TiO_2 NWs as photon anode.

Table 1 Photovoltaics performance of solar cells with 400 nm, 600 nm 900 nm, 1.2 μm TiO_2 NWs as photoanodes.

NW length nm	J_{sc} $mAcm^{-2}$	V_{oc} V	FF	η %	R_{sh} Ω	R_s Ω
400	18.6±0.2	0.85±0.03	0.62±0.03	9.7 ±0.1	1029±22	72 ±5
600	20.4±0.3	0.78±0.02	0.68±0.01	10.8±0.2	1012±20	54 ±8
900	22.3±0.1	0.77±0.02	0.68±0.01	11.7±0.2	1043±16	57 ±5
1200	9.3 ±0.2	0.72±0.02	0.71±0.03	4.8±0.3	957 ±21	114±8

Notes : R_{sh} is Shunt resistance of solar, R_s is series resistance.

The lower shunt resistance of the cells using 1.2 μm TiO_2 NWs than that of the cells using 900 nm NWs indicates a greater charge recombination, resulting in its loss in V_{oc}. The series resistance of the cells using 1.2 μm TiO_2 NWs is notably greater than others due to longer transport distance in 1.2 μm wires.

For comparison, perovskite solar cells using 500 nm thick mesoporous TiO_2 as photoanode are also prepared, which is among the thickness range reported to be the optimized thickness (400 nm - 600 nm) to achieve the best efficiency for mesoporous TiO_2-based cells.[3, 20] We keep all other parameters, such as the coating procedures of peroskite layer, the thickness of the HTM layer and gold layer, the exactly same as the NWs-based cells. As can be seen in Figure S2 in ESI, the V_{oc} of these cells is about 0.80 V, nearly the same as solar cells with TiO_2 NWs as photoanodes. However, the photocurrent of the 500 nm thick mesoporous cells is 14.3 mA/cm^2, about 8 mA/cm^2 lower than the 900 nm NWs-based cells. The efficiency is 6.8% for mesoporous TiO_2 solar cells, which is very close to the reported value (7.16%) for this thickness.[20]

In order to understand the enhancement in J_{sc} found in our 900 nm-long NWs-based devices with respect to the best mesoporous TiO_2-based cells that we can prepare, it is necessary to study their respective light harvesting efficiency (LHE), i.e. external quantum yield, because J_{sc} depends largely on LHE. In Figure S3, it is notable that the device with 900 nm TiO_2 NWs exhibits nearly 95% LHE between 400 nm and 650 nm comparison to 80% in the device with 500 nm mesoporous TiO_2. The LHE for both devices drops after 750 nm, agreeing with literatures.[1, 21, 22]

The fast kinetics of net charge collection in 900 nm-long TiO_2 NWs photoanodes can be evidenced by the photovoltage transient, namely, the kinetic rising profile of V_{oc} of the devices, which reflects how rapidly the electrons and holes can be photoinduced and further transport through the internal layers (electrons from perovskite→TiO_2→FTO, and holes from perovskite→ HTM→gold) in presence of the recombination of the above process.[23] Figure 5 shows that the rising time (defined as the time it takes from shuttle open to 90% of the V_{oc}) of V_{oc} for the 900 nm and 1.2μm long TiO_2 NWs-based perovskite solar cells are 17 ms and 78 ms, respectively. Note that neither the motion of the shutter (response time=0.7ms from full-close to full-open) nor the data acquisition rate (with the highest rate at 10 μs per data point) is the bottleneck of the above measurement, as confirmed by a commercial ultrafast silicon photodiode with a response time of 20 ns (see ESI Figure S 4b). We think the slower photovoltage rising in 1.2 μm NWs is due to the recombination in the thickness that above the maximal hole diffusion length in $CH_3NH_3PbI_3$. Rising time of 400 nm and 600 nm long TiO_2 NWs-based perovskite solar cells are 16.7 ms and 16.9 ms, respectively, as shown in Figure S5. In contrast, rising time of a 500 nm mesoporous anatase film is much slower (see supporting information Figure S 3a).This result agrees with our previous finding that electron transport in TiO_2 rutile NWs-based DSSCs is faster than that in mesoporous films.[17]

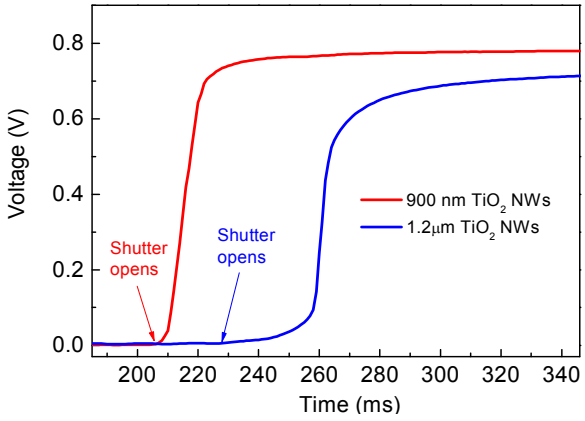

Figure 5. Photovoltage rising transient of devices with 900nm and 1.2μm long TiO_2 NWs photoanodes.

It was reported that thick (over 600 nm) anatase mesoporous TiO_2 layer can cause substantial decrease of FF due to the increment of dark current and electron transport resistance resulting from the convoluted mesoporous pathways,[6] and we obtained the same trend. However, in case of our long (>600 nm) NWs-based perovskite cells, the FF remains over 0.65. For example, the FF of our 900 nm TiO_2 NWs-based cells is 0.68, much better than the corresponding 850 nm thick mesoporous TiO_2-based perovskite cells with FF=0.55. [20]

Conclusions

In summary, length-controllable rutile nanowire arrays with fully accessible and wide-open inter-wire voids are synthesized and used as photoanodes in perovskite solar cells. The length of the NWs reflects a compromise between the thickness of the perovskite material and the effective charge transport in the perovskite material. Due to the high electron diffusivity in rutile nanowires, the electron transport can be effectively conducted in these rutiles nanowires, leaving holes as the majority charge carriers in the perovskite. As a result, effective charge transport can be achieved in up to 900 nm long rutile nanowires, allowing

additional loading of the perovskite materials for higher light absorption, thus, higher attainable current density.

We acknowledge the support from the U.S. National Science Foundation (CBET-1150617), NSFC-21371178 and NSFC-21428305.

Notes and references

[a] Department of Chemistry and Biochemistry, Northern Illinois University, DeKalb, Illinois 60115, USA. *Email: txu@niu.edu
[b] Suzhou Institute of Nano-Tech and Nano-Bionics, Chinese Academy of Sciences, Suzhou, Jiangsu 215123, China. *Email: xjfeng2011@sinano.ac.cn
[c] Xinjiang Institute of Physics & Chemistry, Chinese Academy of Sciences, Urumqi, Xinjiang 830011, China.

Electronic Supplementary Information (ESI) available: e experimental detail, EDS, TEM and XRD, J-V and photovoltage transient of a reference photodioide and a perovskite cell with mesoporous TiO_2 as photoanodes. See DOI: 10.1039/c000000x/

1. A. Kojima, K. Teshima, Y. Shirai and T. Miyasaka, *J Am Chem Soc*, 2009, **131**, 6050-6051.
2. M. Liu, M. B. Johnston and H. J. Snaith, *Nature*, 2013, **501**, 395-398.
3. J. Burschka, N. Pellet, S. J. Moon, R. Humphry-Baker, P. Gao, M. K. Nazeeruddin and M. Gratzel, *Nature*, 2013, **499**, 316-319.
4. J. W. Lee, D. J. Seol, A. N. Cho and N. G. Park, *Adv Mater*, 2014, **26**, 4991-4998.
5. S. D. Stranks, G. E. Eperon, G. Grancini, C. Menelaou, M. J. Alcocer, T. Leijtens, L. M. Herz, A. Petrozza and H. J. Snaith, *Science*, 2013, **342**, 341-344.
6. S. Kazim, M. K. Nazeeruddin, M. Gratzel and S. Ahmad, *Angew Chem Int Ed Engl*, 2014, **53**, 2812-2824.
7. Y. Rong, Z. Ku, A. Mei, T. Liu, M. Xu, S. Ko, X. Li and H. Han, *The Journal of Physical Chemistry Letters*, 2014, **5**, 2160-2164.
8. A. Yella, L. P. Heiniger, P. Gao, M. K. Nazeeruddin and M. Gratzel, *Nano Lett*, 2014, **14**, 2591-2596.
9. M. M. Lee, J. Teuscher, T. Miyasaka, T. N. Murakami and H. J. Snaith, *Science*, 2012, **338**, 643-647.
10. J. Melas-Kyriazi, I. K. Ding, A. Marchioro, A. Punzi, B. E. Hardin, G. F. Burkhard, N. Tetreault, M. Gratzel, J. E. Moser and M. D. McGehee, *Adv Energy Mater*, 2011, **1**, 407-414.
11. A. K. Chandiran, A. Yella, M. T. Mayer, P. Gao, M. K. Nazeeruddin and M. Gratzel, *Adv Mater*, 2014, **26**, 4309-4312.
12. F. Hao, C. C. Stoumpos, D. H. Cao, R. P. H. Chang and M. G. Kanatzidis, *Nature Photonics*, 2014, **8**, 489-494.
13. P. Qin, S. Paek, M. I. Dar, N. Pellet, J. Ko, M. Gratzel and M. K. Nazeeruddin, *J Am Chem Soc*, 2014, **136**, 8516-8519.
14. Z. Zhu, J. Ma, Z. Wang, C. Mu, Z. Fan, L. Du, Y. Bai, L. Fan, H. Yan, D. L. Phillips and S. Yang, *J Am Chem Soc*, 2014, **136**, 3760-3763.
15. J. Qiu, Y. Qiu, K. Yan, M. Zhong, C. Mu, H. Yan and S. Yang, *Nanoscale*, 2013, **5**, 3245-3248.
16. H. S. Kim, J. W. Lee, N. Yantara, P. P. Boix, S. A. Kulkarni, S. Mhaisalkar, M. Gratzel and N. G. Park, *Nano Lett*, 2013, **13**, 2412-2417.
17. X. Feng, K. Zhu, A. J. Frank, C. A. Grimes and T. E. Mallouk, *Angew Chem Int Ed Engl*, 2012, **51**, 2727-2730.
18. N. R. Neale and A. J. Frank, *J Mater Chem*, 2007, **17**, 3216-3221.
19. B. Liu and E. S. Aydil, *J Am Chem Soc*, 2009, **131**, 3985-3990.
20. Y. X. Zhao, A. M. Nardes and K. Zhu, *J Phys Chem Lett*, 2014, **5**, 490-494.
21. J. J. Choi, X. Yang, Z. M. Norman, S. J. Billinge and J. S. Owen, *Nano Lett*, 2014, **14**, 127-133.
22. P. W. Liang, C. Y. Liao, C. C. Chueh, F. Zuo, S. T. Williams, X. K. Xin, J. Lin and A. K. Jen, *Adv Mater*, 2014, **26**, 3748-3754.
23. K. B. Brian C. O'Regan , Jessica Kroeze, Herman Smit, Paul Sommeling, James R. Durrant, *J. Phys. Chem. B*, 2006, **110**, 17155-17160.

